Optical Properties and Electrochemical Dealloying of Gold-Silver Alloy Nanoparticles Immobilized on Composite Thin-Film Electrodes

by

Christopher A. Starr

A Thesis Presented in Partial Fulfillment
of the Requirements for the Degree
Master of Science

Approved March 2014 by the
Graduate Supervisory Committee:

Daniel Buttry, Chair
William Petuskey
Anne Jones

ARIZONA STATE UNIVERSITY

May 2014

ABSTRACT

Gold-silver alloy nanoparticles (NPs) capped with adenosine 5′-triphosphate were synthesized by borohydride reduction of dilute aqueous metal precursors. High-resolution transmission electron microscopy showed the as-synthesized particles to be spherical with average diameters ~4 nm. Optical properties were measured by UV-Visible spectroscopy (UV-Vis), and the formation of alloy NPs was verified across all gold:silver ratios by a linear shift in the plasmon band maxima against alloy composition. The molar absorptivities of the NPs decreased non-linearly with increasing gold content from 2.0×10^8 M^{-1} cm^{-1} (λ_{max} = 404 nm) for pure silver to 4.1×10^7 M^{-1} cm^{-1} (λ_{max} = 511 nm) for pure gold. The NPs were immobilized onto transparent indium-tin oxide composite electrodes using layer-by-layer (LbL) deposition with poly(diallyldimethylammonium) acting as a cationic binder. The UV-Vis absorbance of the LbL film was used to calculate the surface coverage of alloy NPs on the electrode. Typical preparations had average NP surface coverages of 2.8×10^{-13} mol NPs/cm^2 (~5% of cubic closest packing) with saturated films reaching ~20% of ccp for single-layer preparations (1.0×10^{-12} mol NPs/cm^2). X-ray photoelectron spectroscopy confirmed the presence of alloy NPs in the LbL film and showed silver enrichment of the NP surfaces by ~9%. Irreversible oxidative dissolution (dealloying) of the less noble silver atoms from the NPs on LbL electrodes was performed by cyclic voltammetry (CV) in sulfuric acid. Alloy NPs with higher gold content required larger overpotentials for silver dealloying. Dealloying of the more-noble gold atoms from the alloy NPs was also achieved by CV in sodium chloride. The silver was oxidized first to cohesive silver chloride, and then gold dealloyed to soluble $HAuCl_4^-$ at higher potentials. Silver oxidation was inhibited during the first oxidative scan, but

subsequent cycles showed typical, reversible silver-to-silver chloride voltammetry. The potentials for both silver oxidation and gold dealloying also shifted to more oxidizing potentials with increasing gold content, and both processes converged for alloy NPs with >60% gold content. Charge-mediated electrochemistry of silver NPs immobilized in LbL films, using Fc(meOH) as the charge carrier, showed that 67% of the NPs were electrochemically inactive.

ACKNOWLEDGEMENTS

I am grateful to my advisor, Dr. Dan Buttry, for guiding my development as a scientist. He has taught me to be versatile in my scientific approach, and he facilitated my exposure to a wide array of chemistry instrumentation and sub-disciplines. He also challenged my pre-existing perspectives toward critical thinking and encouraged me to approach problems with an open mind. His vast knowledge of scientific literature has exemplified the level of dedication that is needed to excel at research. He was supportive in crises both professional and personal for which I am most thankful. My committee members, Drs. Bill Petuskey and Anne Jones also deserve my gratitude for their technical guidance and personal support.

I am thankful for my colleagues at Arizona State University (ASU) who have supported me both in research and in life. Drs. Harish Bhat and Poonam Singh were always willing to offer a helping hand with experiments or literature, and I valued their friendship. Tim Lamb and Jarred Olson helped me maintain a positive outlook when research challenges seemingly outweighed the successes. David Lowry, Zhenquan Liu, and Dr. Xiaoqian Li provided their assistance with high-resolution transmission electron microscopy, and Tim Karcher assisted with X-ray photoelectron spectroscopy. I acknowledge the use of the facilities in the ASU Leroy Eyring Center for Solid State Science. I thank the National Science Foundation (Grant No. CHE-0957122) for their financial support.

My lifelong gratitude goes to those who have remained closest to me. My wife, Cynthia, has shown unwavering support in challenging times and a willingness to make the best of every situation we encounter. My newborn daughter, Kaitlin, has renewed my

optimism for the future. My parents, Clyde and Kyong, have given me the strength to face challenges rather than avoid them. My family's love has become my source of happiness.

Chapter 2 has been reproduced with permission from Springer Journals as granted in the Copyright Transfer Statement (Appendix A). The original manuscript has been submitted to the Journal of Nanoparticle Research. The DOI number and citation will be provided upon acceptance and online publication. Chapter 3 has been reproduced by permission of ECS - The Electrochemical Society (Appendix B). This article is currently in press with ECS Transactions. The co-author, Dr. Dan Buttry, has consented to the reproduction of both articles.

TABLE OF CONTENTS

Page

LIST OF TABLES vii

LIST OF FIGURES viii

CHAPTER

1 INTRODUCTION 1

2 OPTICAL PROPERTIES OF GOLD-SILVER ALLOY NANOPARTICLES IN SOLUTION AND IN LAYER-BY-LAYER FILMS 4

Introduction 4

Experimental 7

Alloy NP Colloid Synthesis 7

Immobilization of NPs onto Electrode 8

Results and Discussion 10

Conclusions 19

3 ELECTROCHEMICAL DEALLOYING OF GOLD-SILVER NANOPARTICLES - SELECTIVE DISSOLUTION OF THE LESS AND MORE NOBLE SPECIES 20

Introduction 20

Experimental 22

Alloy NP Synthesis and Immobilization 23

Electrochemical Dealloying of NPs 24

Results and Discussion 25

Conclusions 30

CHAPTER Page

4 CHARGE-MEDIATED ELECTROCHEMISTRY OF COMPOSITE NANOPARTICLE THIN-FILMS 32

Introduction....32

Experimental....34

Results and Discussion....35

Conclusions....37

5 SUMMARY....38

REFERENCES....39

APPENDIX

A COPYRIGHT TRANSFER STATEMENT - SPRINGER JOURNALS....43

B PERMISSION TO REPRODUCE OR RE-PUBLISH - ECS JOURNALS....45

LIST OF TABLES

Table Page

1. Optical properties of gold-silver alloy NPs and surface coverages for ITO-PDDA-NP LbL films measured by UV-Vis absorbance 15

2. Elemental composition of ITO-PDDA-alloy NP LbL films quantified from XPS 18

LIST OF FIGURES

Figure Page

1. Representative diagram showing ATP-capped gold-silver alloy NPs immobilized into a 1-layer LbL film on ITO/glass with PDDA cationic binder 6
2. HRTEM images are shown for ATP-$Au_{20}Ag_{80}$ NPs at (a) 1 Mx and (b) 150 kx magnifications with (c) particle diameter histogram ($\bar{x}$ = 4.33 ± 0.82 nm). Also shown are HRTEM images for ATP-$Au_{80}Ag_{20}$ NPs at (d) 150 kx and (e) 1 Mx magnifications with (f) histogram ($\bar{x}$ = 3.44 ± 0.76 nm) 11
3. (a) ATP-Au_xAg_{100-x} NP solutions (conc. 10x) incrementing from pure Ag on the left to pure Au on the right. (b) UV-Vis spectra for ATP-Au_xAg_{100-x} NP solutions (conc. 10x) from synthesis conditions 12
4. The absorbance maxima for NPs in solution (diamonds, R^2 = 0.99) and in LbL films (triangles, R^2 = 0.98) are plotted against alloy composition. The molar absorptivities, ε, for NPs in solution at their λ_{max} are plotted on the secondary (right) y-axis (squares) 14
5. Background-subtracted UV-Vis spectra for LbL films on glass (lighter) and ITO (darker) containing (a) ATP-$Au_{20}Ag_{80}$ NPs, (b) ATP-$Au_{40}Ag_{60}$ NPs, (c) ATP-$Au_{60}Ag_{40}$ NPs, and (d) ATP-$Au_{80}Ag_{20}$ NPs.....16
6. XPS wide spectra for as-prepared ITO-PDDA-NP LbL films containing (a) ATP-$Au_{60}Ag_{40}$ and (b) ATP-$Au_{40}Ag_{60}$ 17
7. Representative diagrams for (a) an alloy NP layer-by-layer (NP-LbL) electrode, (b) electrochemical silver-dealloying of NPs, and (c) electrochemical gold-dealloying of NPs.....21

Figure Page

8. Cyclic voltammograms showing (a) silver-dealloying for $Au_{60}Ag_{40}$ NPs over 5 cycles with silver-dealloying wave enlarged in inset (in 0.1 M H_2SO_4) and (b) the first silver-dealloying scans for the full range of Au_xAg_{1-x} NP compositions (in 0.1 M H_2SO_4) 26
9. Cyclic voltammograms showing (a) gold-dealloying for $Au_{40}Ag_{60}$ NPs over 3 cycles (in 0.1 M NaCl) and (b) the first gold-dealloying cycles for the full range of Au_xAg_{1-x} NP compositions (in 0.1 M NaCl) 29
10. The surface coverages calculated from UV-Vis (diamond) and CV (squares/triangle) are compared showing that a small percentage of NPs are inactive on the LbL film 33
11. Schematic for the charge-mediated oxidation of NPs in LbL films on ITO. The charge-mediator used for this study was Fc(meOH) (E ≈ +200 mV vs. Ag/AgCl)[57] 34
12. The charge-mediated CVs of pure silver NPs in three-layer LbL films and controls on ITO are overlaid. With the exception of the non-mediated AgNP 3-LbL voltammogram which was performed without Fc(meOH), all CVs were performed in 50 mM NaCl and <500 µM Fc(meOH) at a scan rate of 10 mVs^{-1} from -0.6 V to +0.8 V (vs. Ag/AgCl) 36

A1. Copyright transfer statement from Springer journals granting rights to republish to further scientific career in dissertations or similar publications 44
B1. Request for permission to reproduce material that is currently *in press* with *ECS Transaction* in this thesis 46

Chapter 1

INTRODUCTION

Catalysis describes the process where a material increases the rate of a chemical reaction without being consumed in the process, whether it is by passively interacting with the reagents or by regenerating in a secondary process. Despite the ability of catalysts to increase the rate of reactions, they do not affect the total free energy change, and therefore natural spontaneity, of the reaction. Instead, they stabilize the intermediate reaction coordinates and decrease their activation barriers thereby increasing the likelihood that bonding perturbations will proceed to the next reaction coordinate. This ability to speed up nature has made catalysts essential in the industrialized world and has affected the lives of nearly every human being. Some notable examples of impactful catalytic processes are the Haber-Bosch process for dinitrogen fixation for ammonia (fertilizer) production, the hydrogenation of unsaturated hydrocarbons, exhaust catalytic converters, petroleum reforming, and, more recently, proton exchange membrane fuel cells (PEMFCs) and sensors. With the exception of the Haber-Bosch process which uses iron-based catalysts, all of these vital reactions require expensive platinum-group metal catalysts to achieve their maximum performance. Thus, it has become the plight of many materials chemists to identify less expensive alternatives that rival the performance of platinum.

The strategies for designing improved catalysts have often centered around two methodologies. The first involves manipulating the morphology of catalytic materials to influence their surface structure and reactivity. Advancements in nanomaterial

characterization has given scientists better control over material synthesis, so an exceedingly popular strategy for designing catalysts is to reduce the size domain to the nano-scale resulting in increased surface areas, shortened diffusion paths, altered electronic properties including the induction of band gaps in conductive metals, changes in surface unsaturation, and a higher abundance of labile lattice planes at the surface. All of these factors can affect the performance of the catalyst for a given reaction by manipulating their active catalytic sites. A second strategy for catalyst design is the use of promoters, dopants, bimetals, or alloys to extend the library of catalytic materials beyond pure metals or metal oxides. Promoters and dopants are useful for improving catalytic activities by creating isolated, discrete catalytic sites that stabilize multi-step reaction pathways. Bimetals, which have distinct phase boundaries, are attractive for producing cheaper catalysts by replacing an expensive metal in the bulk of the material while leaving the catalytically-relevant metal at the surface with, ideally, unaffected catalytic performance. Bimetals can also behave similarly to promoted catalysts where an isolated secondary reaction step is catalyzed, or it can provide unique catalytic sites at its phase boundaries. Alloys can behave far differently than their pure metal constituents due to the extensive coupling of their electronic states, so alloy composition can provide a variable that allows their catalytic properties to be tuned continuously. Each of these types of catalysts can have positive effects for catalyzing specific reactions depending on the intermediate bonding states along the reaction pathway.

This work reports the use of both aforementioned strategies for designing catalysts by preparing small-scale nanoparticles (NPs) containing alloyed gold and silver and then selectively dissolving away one of the metal species (dealloy) electrochemically

to reduce the NP size dimensions whether by compressive collapse of the NP structure under high surface energies or the induction of nanoporosity. The scope of this project extended to the technical aspects of immobilizing catalytic nanoparticles on conductive electrodes. The optical properties of the alloy NPs were characterized in solution and on transparent composite films to determine their structure, composition, and immobilized surface coverages. Both electrochemical dealloying cases were demonstrated for this gold-silver alloy NP system, and the compositional effects were also discussed qualitatively for silver-dealloying and gold-dealloying. The electroactivities of the NP films were evaluated using charge-mediated electrochemistry to estimate what percentage of NPs were inaccessible by electrons tunneling from the electrode surface. The goal of this research project was to develop a an NP electrode containing small-scale alloy NPs < 5 nm that could undergo further size reduction through dealloying. The underlying motivation was to produce improved electrocatalytic nanomaterials using metals that are more abundant than platinum.

Chapter 2

OPTICAL DETERMINATION OF NANOPARTICLE SURFACE COVERAGES ON LAYER-BY-LAYER THIN-FILM ELECTRODES

Introduction

Alloy nanoparticles (NPs) can show unique optical and catalytic properties compared to their constituent metals.[1-3] Both alloy and bimetallic core-shell NPs have shown improved catalytic performance over pure metallic NPs, demonstrating the significance of surface composition and structure on their activities.[4-7] Decreasing particle size also influences the electrocatalytic behavior of the alloy NPs especially due to increases in coordinatively unsaturated surface sites. Plieth predicted that small NPs (<5 nm) are expected to become increasingly easy to oxidize with decreasing particle radius, again, due to an increasing fraction of surface atoms as size decreases.[8] Gold,[9] silver,[10] and palladium NPs[11] have all been demonstrated to follow the predicted trend. However, this behavior can be complicated in alloy NPs due to surface enrichment by the more noble component during dissolution.[12] The optical properties of noble metal NPs have also been widely examined.[13] They derive from localized surface plasmon resonances (LSPRs) that are affected by size, shape, composition and local dielectric effects.[14] Interestingly, while the qualitative aspects of NP spectral responses have been examined in many papers, there are few examples of quantitative studies that provide important data such as extinction coefficients or molar absorptivities We report here a study of the preparation and optical properties of a series of adenosine-5'-triphosphate

(ATP)-capped gold-silver alloy NPs (ATP-Au_xAg_{100-x} NPs), specifically reporting molar absorptivities for the alloy NPs.

The strategies for gold-silver alloy NP synthesis can employ at least two different approaches. The bottom-up approach describes co-nucleation techniques[15-19] where a mixture of both metal precursors is reduced rapidly to directly form alloy particles with little or no phase-segregation. Preparation of small NPs using this approach typically requires a stabilizing ligand to inhibit particle aggregation.[13] The top-down approach involves galvanic displacement and thermal annealing[4,20-26] where the metals begin phase-separated, and then alloying is induced by interdiffusion. The second approach is facile for producing large alloy NPs, but it is less desirable for producing small NPs because high surface tension could inhibit displacement kinetics and thermal treatment could cause particle growth, aggregation and size polydispersity. Thus, a bottom-up approach becomes the most desirable option for synthesis of small NPs and is employed here. A common synthesis of metallic NPs follows the general scheme originally introduced by Turkevich where colloidal gold NPs form by citrate reduction of a heated tetrachloroauric acid solution.[27] A variation reported by Brook et al.[28] used borohydride as the reductant and ATP as a capping ligand to produce air-stable gold NPs (<6 nm diameter) without heating. This same method was used by our group to synthesize 3.5 – 5 nm diameter silver NPs,[29] and it was chosen for the gold-silver alloy NP synthesis reported here. An important caveat is that the precipitation of highly insoluble silver chloride ($K_{sp} = 1.8 \times 10^{-10}$) in a mixture of gold and silver precursors (typically $AuCl_4^-$ and Ag^+, respectively) has often gone unnoticed and must be avoided. To avoid this,

precursor concentrations were diluted to <10 μM total metals to remain at concentrations where silver chloride precipitation does not occur.[30]

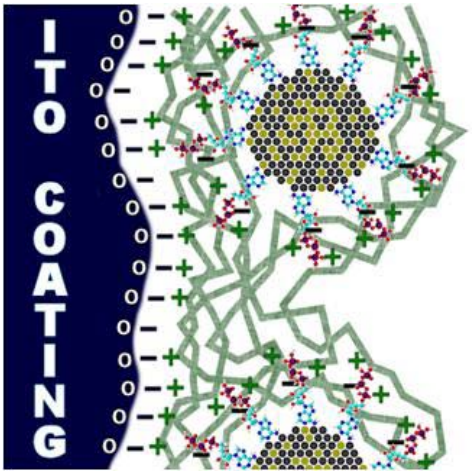

Figure 1. Representative diagram showing ATP-capped gold-silver alloy NPs immobilized into a 1-layer LbL film on ITO/glass with PDDA cationic binder

We also briefly report on incorporation of these alloy NPs into layer-by-layer (LbL) films on glass and indium-tin oxide (ITO) surfaces. Immobilization of NPs onto electrodes has been an active field of study for a variety of applications including catalysis, sensing, bioelectrochemistry, and energy storage. LbL deposition is an interesting approach introduced by Decher[31] in which a composite film is grown by repeatedly depositing oppositely charged materials that are cohesive due to attractive electrostatic interactions. In the present case, poly(diallyldimethylammonium) (PDDA) was chosen to serve as a cationic binder to secure the NPs, which are anionic by virtue of negatively charged ATP adsorbates, with anchoring of the film achieved using PDDA interaction with the negative charges on a properly treated, plasma-etched ITO surface

(Figure 1). Spectroscopy on these LbL films allowed NP surface coverages to be obtained from their plasmon resonance absorbances, demonstrating the value of accurate molar absorptivities in such studies.

Experimental

Alloy NP Colloid Synthesis

Silver nitrate ($AgNO_3$, 99.9+%, Alfa Aesar), tetrachloroauric acid trihydrate ($HAuCl_4 \cdot 3H_2O$, ≥49.0% Au), ATP disodium salt hydrate ($Na_2ATP \cdot xH_2O$, ≥99%), and sodium borohydride ($NaBH_4$, ≥98.5%) were purchased from Sigma-Aldrich. All solutions were prepared using 18.2 MΩ deionized (DI) water from a Millipore MilliQ purification system. An inert atmosphere was used to avoid the oxidation of the particles during or after synthesis, prior to isolation. The reaction flask was sealed under N_2 flow through high-density polyethylene (HDPE) tubing into o-ring-gasketed gas inlet/outlet tubes terminating into a mineral oil backflow trap. Precursor solutions were prepared using N_2-purged DI water and injected into the flask by syringe through a rubber septum.

The reaction flask was filled with 400 mL DI water, sealed, and N_2 was bubbled in under constant stirring. After at least 20 min, the N_2 inlet was raised to redirect gas flow above the solution for the remainder of the synthesis. Stock $AgNO_3$ (0.709 mM) and $HAuCl_4$ (0.709 mM) solutions were added at varying ratios depending upon the desired alloy NP composition to a combined volume of 5.0 mL (8.5 μM total metals concentration). These dilute concentrations were necessary to avoid the loss of Ag^+ by precipitation of AgCl. A fresh ATP solution (3.5 mM, 5.0 mL) was added in 5-fold molar excess of the metal precursors to serve as the capping ligand. The clear solution

continued stirring for 20 minutes at room temperature to allow thorough mixing. Then, fresh $NaBH_4$ (20 mM, 5.0 mL) reducing agent was rapidly injected under stirring. This resulted in an immediate color change from the pale yellow due to the $HAuCl_4$ precursor to a range of colors depending on the gold:silver ratio. Stirring was stopped after 30 min, and typically left to equilibrate overnight (~18 h). These syntheses appear to proceed with very high yields; under no circumstances was residue observed after NP formation. Thus, all of the metal precursors added to the synthetic solution are reduced and contribute to the formation of the metallic NPs.

The capped-NP solutions were disconnected from N_2 flow, immediately transferred to a rotary evaporator and concentrated to <40 mL under vacuum in a 38ºC heated bath. A portion was reserved before evaporation for UV-Vis analysis. The resulting solution was diluted to 40 mL (conc. 10x) with DI water and stored in capped vials for use in LbL film preparations. UV-Visible spectroscopy (UV-Vis) of NP solutions were carried out on a Cary 50 UV-Vis spectrophotometer in 1-cm path length quartz cuvettes. High-resolution transmission electron microscopy (HRTEM) samples were prepared by micropipette drop-wick-evaporation of the concentrated solutions onto 300-mesh Formvar-coated Cu grids. Images were obtained using a JEOL 2010F field emission transmission electron microscope at 200 kV accelerating voltage. ImageJ v1.45s software was used to produce size dispersion histograms.

Immobilization of NPs onto Electrode

ITO-coated borosilicate glass slides (Delta Technologies, Ltd., 5-15Ω, >85% transmittance) were cleaned by sonication for 20 min each in isopropyl alcohol (IPA,

99.9%, Sigma-Aldrich) and DI water. After another DI water rinse and drying by N_2 flow, the slides were plasma-etched in air at 6 mbar for 5.0 min (Edwards E306A thermal evaporative coater). The slides were quickly removed and the lower portion (7 × 10 mm) of each slide was immediately immersed into a capped 1 mg/mL solution of PDDA chloride ($M_{w(avg.)}$ = 200,000-350,000, Sigma-Aldrich) cationic polymer for 30 minutes. They were then immersed in the evaporated, concentrated alloy NP solution for at least 30 min followed by the PDDA solution again for 20 min with a DI water rinse between each step. After a final rinsing, the resulting ITO-PDDA-NP LbL slides were dried completely over N_2 flow before analysis. Only one LbL NP layer was deposited, although a PDDA top-layer was applied to further stabilize the NPs by encapsulation in the film.

XPS was used to characterize the LbL films. Samples for XPS analysis were prepared with higher NP coverages (~16 h soaking in NP solutions during LbL preparation) to enhance the XPS signals. NP-saturated LbL samples intended for surface coverage calculations were immersed in alloy NP solution >24 h. Data were collected using a VG ESCALAB 220i-XL photoemission spectrometer with a monochromated Al kα source (65 W) under ultrahigh vacuum (UHV) < 10^{-9} torr. The binding energies were calibrated using adventitious carbon as a reference. CasaXPS software v2.3 was used for quantitative analysis. UV-Vis of ITO-PDDA-NP and Glass-PDDA-NP LbLs were measured on the Cary 50 UV-Vis spectrophotometer by securing slides perpendicular to the source beam. Subtraction of the ITO background was done individually for each slide due to the slight variations observed in their spectra. Surface coverage of NPs was calculated from background-corrected absorbances using $A = \varepsilon' \Gamma$, where ε' ($cm^2\ mol^{-1}$)

is a “surface” molar absorptivity derived from the solution phase molar absorptivity, ε (M^{-1} cm^{-1}), using ε’ = ε (10^3).

Results and Discussion

The synthesis produced stable, aqueous ATP-Au_xAg_{100-x} NPs with relatively monodisperse particle size distributions. Characterization data for a few selected compositions are provided. Figure 2 shows HRTEM images for typical alloy NP syntheses with accompanying particle diameter histograms. Both silver-rich ATP-$Au_{20}Ag_{80}$ NPs and gold-rich ATP-$Au_{80}Ag_{20}$ NPs had similar average particle diameters of ~4 nm, suggesting that their alloy compositions did not significantly affect the size of the as-synthesized NPs. As seen in Fig. 2, twinning defects were visible in the high-magnification images of both alloy NP compositions. This was likely due to a growth-aggregation mechanism for NP formation[32,33] rather than a phase boundary in the alloy. This conclusion is supported by energy-dispersive X-ray absorbance spectroscopy (EDX) studies using scanning-mode TEM on similarly produced gold-silver NPs showing uniform alloy composition in individual NPs.[34] Both ATP-Au NPs and ATP-Ag NPs have face-centered cubic (FCC) structure[28,35] and nearly identical bulk lattice constants (a_{Au} = 4.08 Å, a_{Ag} = 4.09 Å),[36] so powder X-ray diffraction (PXRD) was not useful in distinguishing alloy composition. The synthesis was successful in producing NPs in the desired size range, and the considerably dilute conditions resulted in highly dispersed NPs.

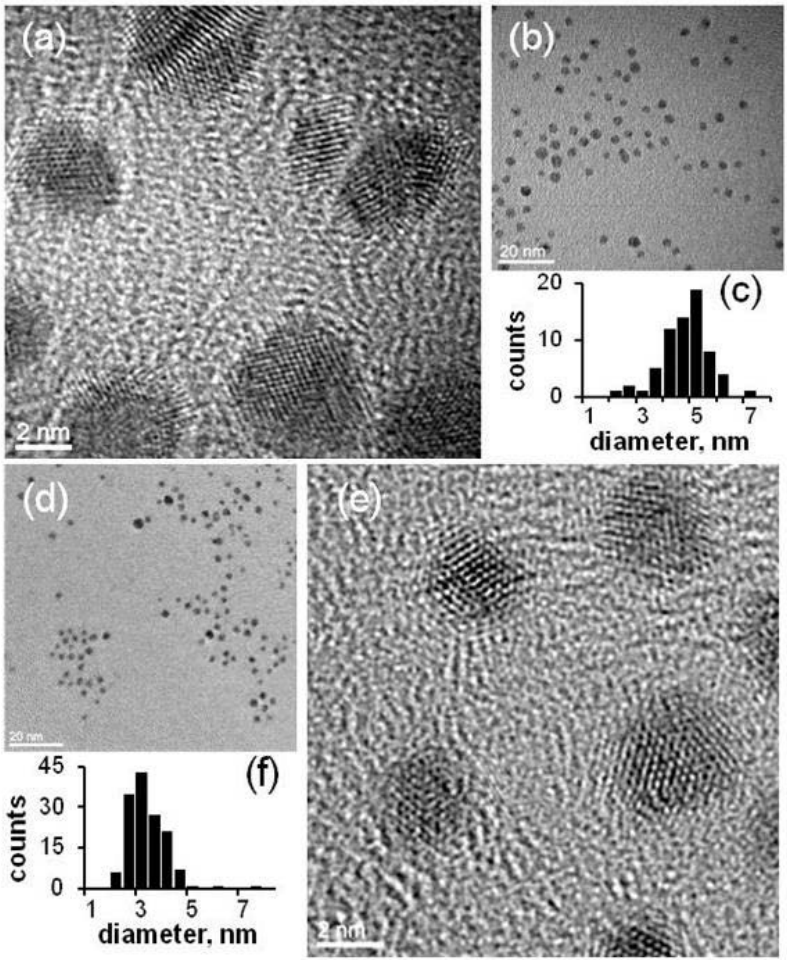

Figure 2. HRTEM images are shown for ATP-$Au_{20}Ag_{80}$ NPs at (a) 1 Mx and (b) 150 kx magnifications with (c) particle diameter histogram ($\bar{x}$ = 4.33 ± 0.82 nm). Also shown are HRTEM images for ATP-$Au_{80}Ag_{20}$ NPs at (d) 150 kx and (e) 1 Mx magnifications with (f) histogram ($\bar{x}$ = 3.44 ± 0.76 nm)

The successful alloying of gold and silver in the NPs was confirmed from the continuous shift of the LSPR bands of the alloy NP solutions between those of the pure (end member) metals. This trend has been previously reported for other gold-silver alloy NP systems.[15,16,25,37] LSPR absorbance is caused by oscillations in the electron density of

nanoscale conducting particles at a dielectric interface. For ATP-Au_xAg_{100-x} NP solutions, the LSPR was observed in the visible range. Prior to reduction, the reaction solution had a very faint yellow tint due to the $HAuCl_4$ precursor. Upon reduction by borohydride, the solution immediately changed color confirming the nucleation of plasmonic NPs had occurred. The color underwent further subtle changes as the NPs grew and stabilized. The final color of the alloy NP solutions varied from bright yellow to pale red depending on their composition (Figure 3a).

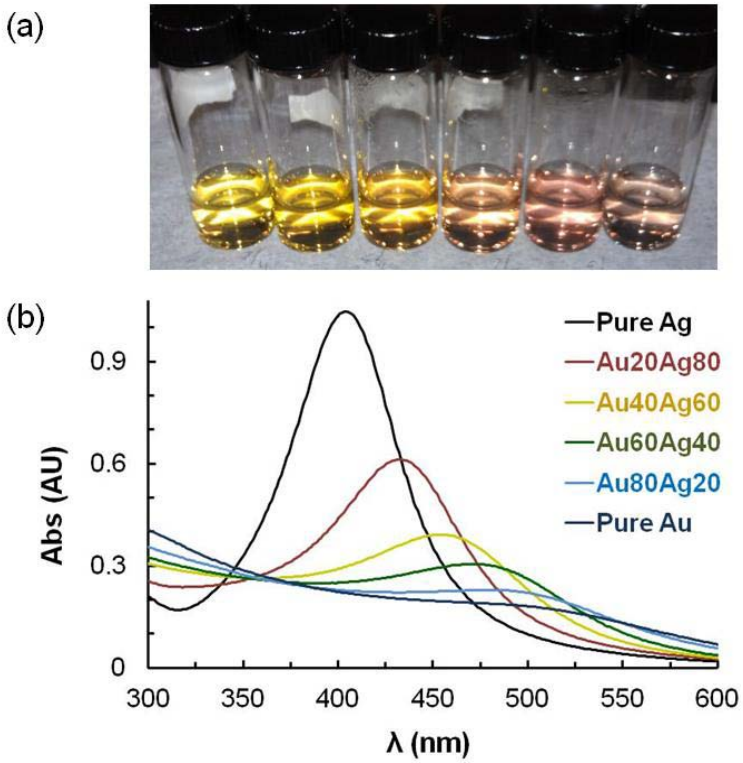

Figure 3. (a) ATP-Au_xAg_{100-x} NP solutions (conc. 10x) incrementing from pure Ag on the left to pure Au on the right. (b) UV-Vis spectra for ATP-Au_xAg_{100-x} NP solutions (conc. 10x) from synthesis conditions

The trend in LSPR absorbance intensity and λ_{max} was measured by UV-Vis for the ATP-Au_xAg_{100-x} alloy NP solutions (Figure 3b). Pure ATP-Au NPs had a weak absorbance at 511 nm on a sloping background profile, pure ATP-Ag NPs had a strong absorbance at 404 nm, and the intermediate alloy compositions showed gradual shifts in peak absorbance and intensities between these limits. The presence of only one LSPR peak for each spectrum and the regular trend in intensity and λ_{max} showed that NP composition in a sample was homogeneous rather than a mixture of gold-rich and silver-rich NPs.[22,37] The lack of a shoulder or secondary LSPR peaks also confirmed that phase-separated, core-shell structures were not formed.[24,38-40] The LSPR λ_{max} values of the alloy NPs shifted linearly with the gold:silver ratios used in the synthesis solutions (Figure 4) verifying that an alloy had formed at all compositions. The λ_{max} values of the alloys did not deviate from the linear regression between pure gold and pure silver, also suggesting that Au and Ag had formed alloy NPs efficiently without loss of either metal during the synthesis.

Molar absorptivities (on a moles of NP per volume basis) at the λ_{max} were calculated for each alloy NP composition using an average NP diameter of 4.0 nm and assuming that all precursor metals reacted completely to form NPs (see Experimental). As seen in Figure 4 (squares), the molar absorptivities (ε) of the NPs varied non-linearly but monotonically from 2.0×10^8 M^{-1} cm^{-1} for ATP-Ag NPs to 4.1×10^7 M^{-1} cm^{-1} for ATP-Au NPs (Table 1). These values may be compared with a very limited number of previous reports of ε values. Molar absorptivities reported by El Sayed and coworkers[15] for citrate-capped gold-silver alloy NPs that were 20 nm in diameter showed a similar

trend of (nearly) exponentially decreasing ε with increasing Au mole fraction in the alloy NP. However, the values reported by El-Sayed and coworkers were uniformly larger, for example, reporting a value of 1.0×10^9 M^{-1} cm^{-1} for 20 nm diameter pure gold NPs. These larger values are likely characteristic of their larger NP diameters. The present values are more similar to those for citrate-capped gold NPs reported by Huo et al. ($\varepsilon = 0.856 \times 10^7$ M^{-1} cm^{-1} for 4.6 nm diameter NPs).[41] Their results also showed a substantial decrease in molar absorptivity with decreasing size. This is consistent with the different molar absorptivities for the larger NPs studied by El-Sayed and coworkers, the smaller ones studied by Huo et al. and those reported here. The two evident trends are that larger NPs have larger molar absorptivities and that molar absorptivity decreases as Au mole fraction increases through a series of alloys.

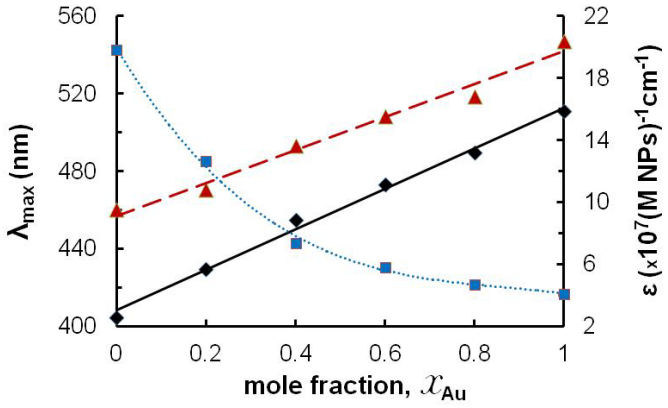

Figure 4. The absorbance maxima for NPs in solution (diamonds, $R^2 = 0.99$) and in LbL films (triangles, $R^2 = 0.98$) are plotted against alloy composition. The molar absorptivities, ε, for NPs in solution at their λ_{max} are plotted on the secondary (right) y-axis (squares)

Table 1. Optical properties of gold-silver alloy NPs and surface coverages for ITO-PDDA-NP LbL films measured by UV-Vis absorbance

χ		λ_{max} (nm)			ε (NP)	Γ (NP)
Au	Ag	sol'n	LbL	Δ	($M^{-1}cm^{-1}$)	(mol cm^{-2})[a]
0.00	1.00	404	460	+56	20×10^{7}	1.9×10^{-13}
0.20	0.80	430	470	+40	13×10^{7}	2.4×10^{-13}
0.40	0.60	455	493	+38	7.4×10^{7}	4.5×10^{-13}
0.60	0.40	473	509	+36	5.8×10^{7}	3.9×10^{-13}
0.80	0.20	490	519	+29	4.7×10^{7}	3.6×10^{-13}
1.00	0.00	511	547	+36	4.1×10^{7}	0.48×10^{-13}

[a] *~30 min NP sol'n immersion time for LbL, conc. 10x*

To demonstrate the value of molar absorptivity data, the optical properties of these gold-silver alloy NPs were used to calculate NP surface coverages in LbL films. Upon deposition into LbL films (on both glass and ITO), the LSPR λ_{max} values of the alloy NPs were red-shifted by changes in the localized dielectric environment by an average of +39 nm (Figure 5). The interactions responsible for this shift are not fully understood, but its prevalence on glass substrates suggested it was not due to interactions with the ITO. A similar shift was also observed by Zhong et al.[42] on various substrates. They attributed this to interactions between adjacent NPs immobilized in LbL films.[43] However, TEM images of PDDA-ATP-AgNP LbL films have confirmed that particles do not aggregate during film deposition.[29] Because of this lack of aggregation, it was assumed that the LSPR absorptivity would remain similar despite the small red-shift in energy, allowing the use of solution phase molar absorptivities for calculating surface coverages on ITO and glass.

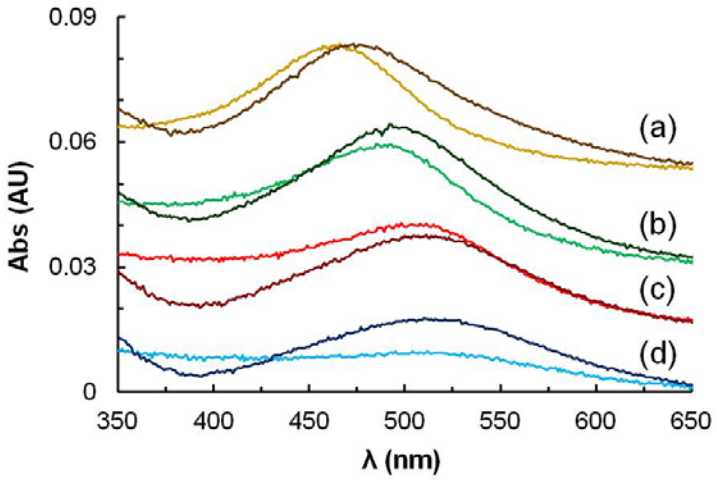

Figure 5. Background-subtracted UV-Vis spectra for LbL films on glass (lighter) and ITO (darker) containing (a) ATP-$Au_{20}Ag_{80}$ NPs, (b) ATP-$Au_{40}Ag_{60}$ NPs, (c) ATP-$Au_{60}Ag_{40}$ NPs, and (d) ATP-$Au_{80}Ag_{20}$ NPs

Surface coverages were calculated using background-corrected absorbances for NPs in LbL films and solution phase molar absorptivities (see Experimental). The validity of this approach was supported by comparisons to thickness measurements using quartz crystal microbalance (QCM) and atomic force microscopy (AFM).[42,43] The UV-Vis absorbance of the alloy NP films was measured after 30 min immersion time in the NP solution during the LbL preparation. Surface coverages from this preparation are listed in Table 1. These films had sub-monolayer surface coverages, Γ, with an average Γ of 2.8×10^{-13} mol NPs/cm^2 (~5% of cubic closest packing (ccp)). This low coverage also supports the assumption that interparticle interactions would not strongly affect the molar absorptivity. Saturated films (>24 h in NP solution for LbL) had coverages as high as 1.0

$\times 10^{-12}$ mol NPs/cm^2 (~20% of ccp), so complete monolayer deposition was not achieved even for highly loaded films.

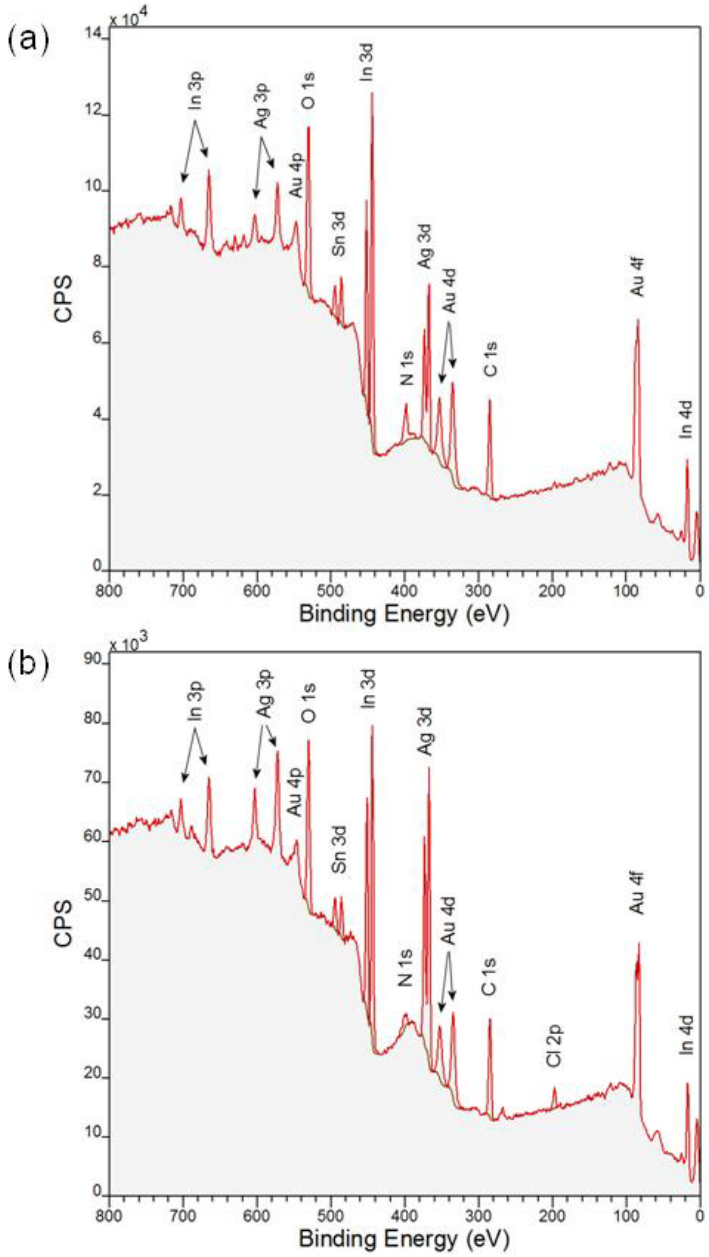

Figure 6. XPS wide spectra for as-prepared ITO-PDDA-NP LbL films containing (a) ATP-$Au_{60}Ag_{40}$ and (b) ATP-$Au_{40}Ag_{60}$

Table 2. Elemental composition of ITO-PDDA-alloy NP LbL films quantified from XPS

at%	Au 4d	Ag 3d	In 3d	Sn 3d	O 1s	C 1s	N 1s	Cl 2p	x_{Au}	x_{Ag}	$\Delta\%_{Ag}$
ATP-$Au_{60}Ag_{40}$	5.39	5.33	8.50	1.05	25.36	41.06	13.31	--	0.503	0.497	+9.7
ATP-$Au_{40}Ag_{60}$	4.61	9.68	8.37	1.02	24.97	42.04	5.82	3.48	0.323	0.677	+7.7

The immobilization of alloy NPs was confirmed in the XPS wide spectra of ITO-PDDA-NP LbL films (Figure 6). This surface-sensitive technique provides elemental composition of the sampled surface within a shallow 1-2 nm electron escape depth. The relative abundances of each element in the films were quantified and are given in Table 2. The gold and silver signals from the alloy NPs were clearly visible above the ITO background verifying that alloy NPs were retained on the electrode despite washing after LbL preparation. The gold:silver ratios detected by XPS showed a higher abundance of silver in both gold-rich and silver-rich alloy NPs compared to their expected composition from LSPR by an average of ~9%at. This surface enrichment of silver in gold-silver alloy NPs has been observed in other experimental gold-silver alloy NP studies.[37,44] Interestingly, despite evidence of a slight surface enrichment in Ag, the LSPR λ_{max} values did not deviate from a linear dependence on the alloy composition.

Conclusions

Spherical ATP-capped gold-silver alloy NPs with average diameters ~4 nm were synthesized from a one-pot aqueous method. The alloying of gold and silver in the NPs was confirmed by a linear shift of the LSPR λ_{max} in their UV-Vis spectra as a function of alloy composition. Molar absorptivities for the alloy NP solutions were calculated from the spectra. The results described here provide one of only a very few sets of molar absorptivity values for gold-silver alloy NPs. They are consistent with past data showing that smaller NPs have smaller molar absorptivities and that the molar absorptivity decreases as the mole fraction of Au in the NP is increased. The NPs were immobilized into ITO-PDDA-NP LbL films. XPS showed surface enrichment of silver in both silver-rich and gold-rich alloy NPs. Molar absorptivities of the alloy NPs were used to calculate their surface coverages on ITO in the LbL films, showing that surface coverages obtained using the loading procedures employed here give ~ 5% of monolayer coverage, revealing the value of using quantitative molar absorptivities for such measurements.

Chapter 3

ELECTROCHEMICAL DEALLOYING OF GOLD-SILVER NANOPARTICLES

Introduction

Dealloying has been studied extensively for its relevance to industrial corrosion, but more recently it has been used to produce unique nanomaterials with applications in electrocatalysis. Noble metal alloys themselves have garnered interest for their tunable surface properties and potential to replace expensive platinum-group metals in reduction catalysts.[45,46] Thus, controlled dealloying of catalytically-relevant systems has also been utilized to further modify their active surface sites and improve their activities.[4,47-49] Most studies have focused on bulk alloys where the high surface mobilities of the metal atoms allow extensive pitting to penetrate the bulk. For bulk gold-silver alloys, Sieradzki et al. showed that chemical silver-dealloying with nitric acid carved intricate nanoporous gold (NPG) structures with large surface areas that showed exceptional catalytic performance.[50-53] Interestingly, Ma et al. also demonstrated a "reverse" dealloying case for bulk gold-silver where thiourea was used to selectively etch gold from the lattice. Similarly, this technique created highly-ligamented silver nanoporous structures.[54] Far fewer studies have shown dealloying in nanoparticles (NPs), particularly small-scale NPs <10 nm, where non-trivial surface energies and shortened diffusion paths for the passivating metal might inhibit dealloying. Experimental data for electrochemically dealloying gold-silver alloy NPs were not located in the literature. Monte Carlo simulations predicted that dealloying could still overcome curvature effects in gold-silver alloy NPs as small as 4 nm in diameter by applying an overpotential to increase the silver

etch rate above the diffusion rate of passivating gold atoms to the etch front.[12] Successfully dealloying small-scale NPs could lead to porous NPs or collapsed NPs with reduced size dimension and interesting catalytic properties. Thus, it becomes useful to demonstrate the dealloying of gold-silver alloy NPs experimentally.

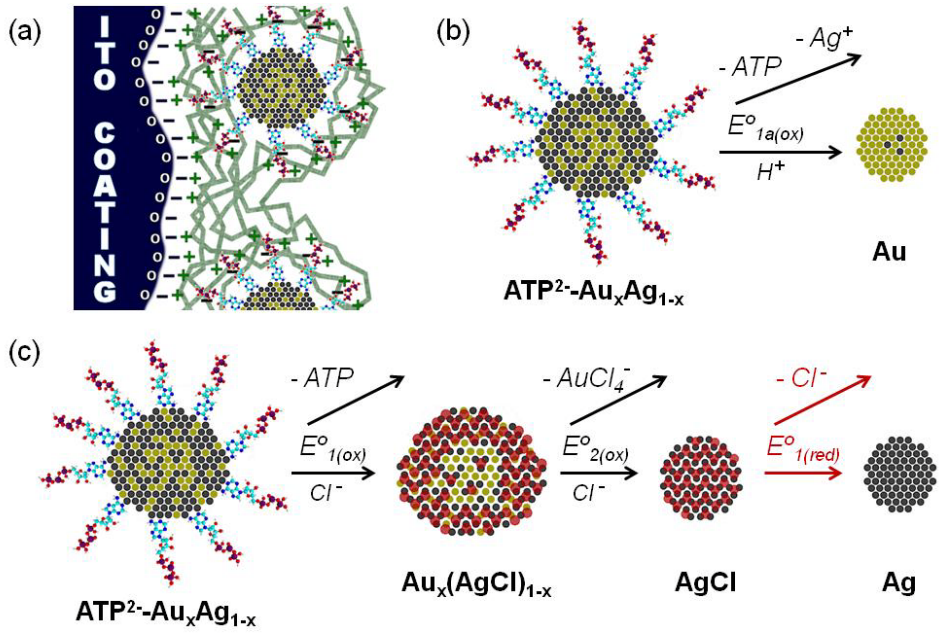

Figure 7. Representative diagrams for (a) an alloy NP layer-by-layer (NP-LbL) electrode, (b) electrochemical silver-dealloying of NPs, and (c) electrochemical gold-dealloying of NPs

Here we report the electrochemical dealloying of gold-silver alloy NPs with average diameters of ~4 nm immobilized on a composite indium-tin oxide electrode (ITO) using layer-by-layer (LbL) deposition (Figure 7). The preparation of gold-silver alloy NPs and NP-LbL electrodes followed established methods[28,31] which had been further optimized and characterized by this group.[55] Straightforward silver-dealloying

was performed using cyclic voltammetry (CV) in sulfuric acid where silver was oxidized to Ag^+ below the onset potential for gold oxidation. The silver(I) ions irreversibly dissolved away from the lattice while gold atoms were retained as NPs. We also demonstrated the "reverse" dealloying case for gold-silver alloy NPs where gold was selectively etched from the NPs. This was performed by CV in sodium chloride where silver oxidized first to cohesive silver chloride which allowed gold to be oxidized to soluble tetrachloroaurate ion at higher potentials. The relevant thermodynamic potentials for each process are listed in equations [1-3]. Both dealloying cases were performed for the full range of alloy NP compositions to allow a qualitative discussion of how composition affected their dealloying behavior.

$$Ag^+ + e^- \rightleftharpoons Ag \qquad (E_{1a} = 0.58 \text{ V vs. Ag/AgCl}) \qquad [1]$$

$$AgCl + e^- \rightleftharpoons Ag^+ + Cl^- \qquad (E_1 = 0.00 \text{ V vs. Ag/AgCl}) \qquad [2]$$

$$AuCl_4^- + 3\ e^- \rightleftharpoons Au + 4\ Cl^- \qquad (E_2 = 0.78 \text{ V vs. Ag/AgCl}) \qquad [3]$$

Experimental

Silver nitrate ($AgNO_3$, 99.9+%, Alfa Aesar), tetrachloroauric acid trihydrate ($HAuCl_4 \cdot 3H_2O$, ≥49.0% Au), adenosine 5'-triphosphate disodium salt hydrate ($Na_2ATP \cdot xH_2O$, ≥99%), sodium borohydride ($NaBH_4$, ≥98.5%), sulfuric acid (H_2SO_4, 95-98%), isopropyl alcohol (IPA, 99.9%), and poly(diallyldimethylammonium chloride) (PDDA, $M_{w(avg.)}$ = 200,000-350,000) were purchased from Sigma-Aldrich. Sodium chloride (≥99.0%, Mallinckrodt) was purchased from VWR. ITO-coated borosilicate glass slides (5-15Ω, >85% transmittance) were purchased from Delta Technologies, Ltd.

All NP and electrolyte solutions were prepared using 18.2 MΩ deionized (DI) water (Millipore MilliQ purification system).

Alloy NP Synthesis and Immobilization

In a typical alloy NP synthesis, 400 mL DI water was sealed by septa into a round-bottom flask under constant stirring and positive-pressure N_2 flow into a mineral oil backpressure trap. Stock $AgNO_3$ (0.709 mM) and $HAuCl_4$ (0.709 mM) solutions were injected by syringe at varying ratios to achieve the desired alloy NP composition to a combined volume of 5.0 mL. These dilute concentrations prevented the sacrificial loss of Ag^+ to AgCl precipitation ($K_{sp} = 1.8 \times 10^{-10}$) upon the addition of $HAuCl_4$. A fresh Na_2ATP capping-ligand solution (3.5 mM, 5.0 mL) was added in 5-fold molar excess over the total metals concentration. The pale-yellow solution continued stirring for 20 minutes at room temperature, and then an excess of fresh $NaBH_4$ (20 mM, 5.0 mL) reducing agent was rapidly injected by syringe. This caused an immediate color change from pale red to bright yellow for pure gold and pure silver, respectively. This confirmed that plasmonic nanocluster nucleation had occurred. Stirring was stopped after 30 min, and NP growth-aggregation and capping proceeded for ~18 h. The solutions were then unsealed from N_2 flow and transferred to a rotary evaporator (rotovap) and concentrated to ~40 mL under vacuum at 38ºC.

For the NP-LbL electrode preparation, ITO-coated borosilicate glass slides were cleaned by sonication in isopropyl alcohol and DI water for 20 min each and dried by N_2 flow. The slides were then plasma-etched in ambient air (6 mbar) for 5 min to deprotonate the ITO surface (Edwards E306A thermal evaporative coater). The slides

were quickly removed and the lower portion (7 x 10 mm) of each slide was immersed into individual 1 mg/mL solutions of PDDA cationic polymer for 30 min. They were then rinsed with DI water and transferred to rotovap-concentrated alloy NP solutions for 1 h. A final layer of PDDA was deposited by immersing for 20 min. After a final rinse with DI water, the NP-LbL electrodes were dried completely over N_2 flow before their use in electrochemical experiments.

Electrochemical Dealloying of NPs

Cyclic voltammetry (CV) was used to show the dealloying behavior of the gold-silver alloy NP-LbL electrodes. All electrochemical measurements were performed with a CHI760C potentiostat (CH Instruments, Inc.) using a flame-polished Pt folded-wire counter electrode and Ag/AgCl (saturated NaCl) reference electrode (+0.22 V vs. SHE). Electrolyte solutions were purged with N_2 for at least 20 minutes before any electrochemical experiments. The potentiostat leads were clipped to a gold foil folded over the top of the NP-LbL electrode and kept dry.

Ag-dealloying was performed in 0.1 M H_2SO_4. Fresh electrolyte was used for each run and the AgCl reference electrode was immersed immediately prior to scans to prevent significant Cl^- from leaching into the cell. The NP-LbL electrode was held at -0.1 V for 4 s and then cycled between -0.1 V and +0.9 V at 10 mV/s scan rate for 4 cycles. On the 5th cycle, the scan was extended to higher oxidative potentials from -0.1 V to +1.4 V. Au-dealloying of NP-LbL electrodes occurred in 0.1 M NaCl. After a 4 s hold time at -0.3 V, the electrode was cycled between -0.3 V and +1.0 V at a scan rate of 10 mV/s for 4 cycles.

Results and Discussion

The electrochemical dealloying of silver from alloy NP-LbL electrodes containing $Au_{60}Ag_{40}$ NPs was performed by CV (Figure 8a). An acidic electrolyte was used to allow direct oxidation of silver to Ag^+ at potentials below the oxidation of gold to $Au(OH)_3$. The particles were first held at a reducing potential of -0.1 V (vs. Ag/AgCl) for 4 s to remove any possible surface passivation, and then an oxidative scan was applied from -0.1 V to +0.9 V at 10 mV/s to selectively etch away the silver from the NPs over 5 cycles. Silver oxidation occurred at an onset potential of +0.32 V and reached a broad peak at +0.74 V. With the exception of a subtle wave during the first cycle, the lack of a silver-reduction wave during return scans showed that Ag^+ was irreversibly dissolving out of the NPs. Upon cycling, the silver-dealloying wave decreased as silver was removed until only a small change was observed by the fourth cycle. On the fifth cycle, the scan was extended to a higher oxidative potential of +1.4 V to confirm the presence of gold NPs remaining in the NP-LbL electrode by reversibly oxidizing it to $Au(OH)_3$. Integrating the silver-dealloying (1 e^-) and gold-oxidation (3 e^-) peaks gave a calculated NP composition of 57.9% Au and 42.1% Ag which correlated well with the as-synthesized NP composition of 60% Au and 40% Ag. Continued research to characterize the structure and composition of dealloyed NPs is ongoing.

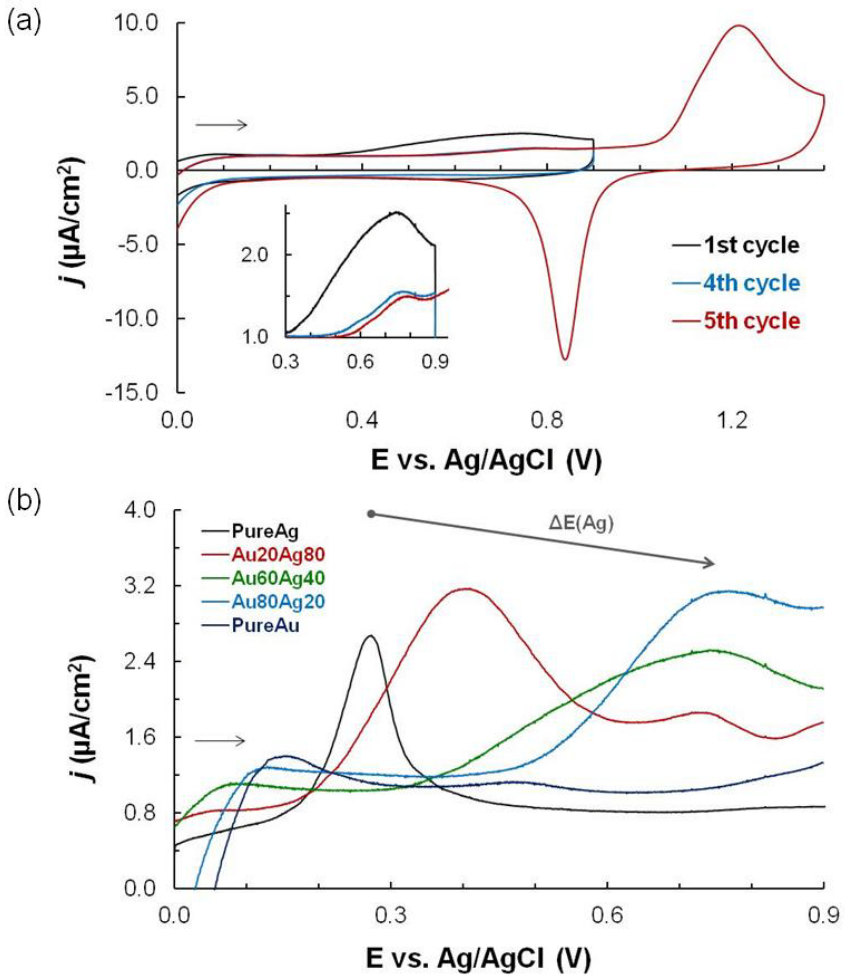

Figure 8. Cyclic voltammograms showing (a) silver-dealloying for $Au_{60}Ag_{40}$ NPs over 5 cycles with silver-dealloying wave enlarged in inset (in 0.1 M H_2SO_4) and (b) the first silver-dealloying scans for the full range of Au_xAg_{1-x} NP compositions (in 0.1 M H_2SO_4)

The alloy NP composition influenced their silver-dealloying behavior where higher gold content inhibited the oxidation of silver , pushing the process to larger overpotentials. The first scans for silver-dealloying are shown for samples spanning the full range of alloy compositions (Figure 8b). Silver-dealloying in $Au_{20}Ag_{80}$ NPs began at +0.14 V (vs. Ag/AgCl) which was similar to pure silver NPs, however, the dealloying

wave was broader and peaked 134 mV higher. A smaller, secondary silver-oxidation wave with an onset potential of +0.64 V was also observed. It was possible that in these silver-rich NPs, most of the silver atoms dealloyed easily at a low overpotential until particle dimensions were etched down to a size where the sparse gold atoms could diffuse to the etch front. Thus, the secondary peak in the voltammetry of silver-rich $Au_{20}Ag_{80}$ NPs may have been caused by a small subset of silver atoms that were protected by gold in the NP cores. As hypothesized by Sieradzki et. al., dealloying could overcome this blocking by applying an overpotential that could increase the silver etch rate above the diffusion rate of passivating gold atoms. They also showed that this critical dealloying potential shifted more oxidizing for alloys with higher gold content due to the abundance of gold atoms to block silver in the bulk.[56] In our alloy NPs, the onset of silver-dealloying also shifted to higher potentials for gold-rich NPs at +0.31 V and +0.44 V for $Au_{60}Ag_{40}$ and $Au_{80}Ag_{20}$, respectively. Contrary to expectations, the shortened diffusion paths and high surface energies in these alloy NPs did not result in significant increases in the overpotential for silver-dealloying compared those reported for the bulk alloy.

"Reverse" dealloying of more noble gold atoms from alloy NP-LbL electrodes was achieved by CV in chloride. The silver atoms were retained as cohesive NPs in their oxidized state as insoluble silver chloride which allowed gold to be dealloyed as soluble tetrachloroaurate ion at higher oxidative potentials. The voltammogram for gold-dealloying is shown for $Au_{40}Ag_{60}$ NPs (Figure 9a). The NPs were first held at a reducing potential of -0.3 V (vs. Ag/AgCl) for 4 s and then cycled between -0.3 V to +1.0 V. In the first oxidative scan, silver-oxidation was inhibited with an onset at +0.15 V. This inhibition suggested that gold stabilized the silver atoms in the NPs. Inhibition from the

coupled release of the capping ligand was not likely as similar ATP-capped NPs in a previous study did not exhibit an overpotential for silver oxidation in chloride.[29] The irregular silver-oxidation wave showed two distinct processes centered at +0.36 V and +0.53 V. This separation in the silver-oxidation wave suggested that silver atoms were present in two predominant electronic states in the alloy NP. It was possible the first state was labile silver atoms at the NP surface and the more noble state was silver atoms highly-coordinated to gold in the NP cores. Conversely, silver-coordination had a destabilizing effect on gold atoms as the gold-dealloying onset at +0.6 V was below its thermodynamic potential (equation [3]). But similarly, gold-dealloying was separated into two discrete oxidation processes peaking at +0.70 V and +0.82 V. This also was likely due to labile surface atoms and protected core atoms. The first return scan showed only a small gold-reduction peak from recaptured $AuCl_4^-$ starting at +0.60 V followed by a large silver-reduction wave for retained AgCl NPs at 0 V. Reversible silver-to-silver chloride electrochemistry appeared in the second cycle and persisted at its thermodynamic potential in subsequent cycles. This showed that silver NPs were successfully retained in the NP-LbL electrode after gold-dealloying. The gold-dealloying peak was smaller in the second scan and absent in the third scan signifying gold-dealloying had completed within 3 cycles, and no additional $AuCl_4^-$ was redeposited in subsequent return scans. Ratios for Au:Ag could not be calculated from the voltammogram due to the convolution of the silver-dealloying and gold-dealloying peaks.

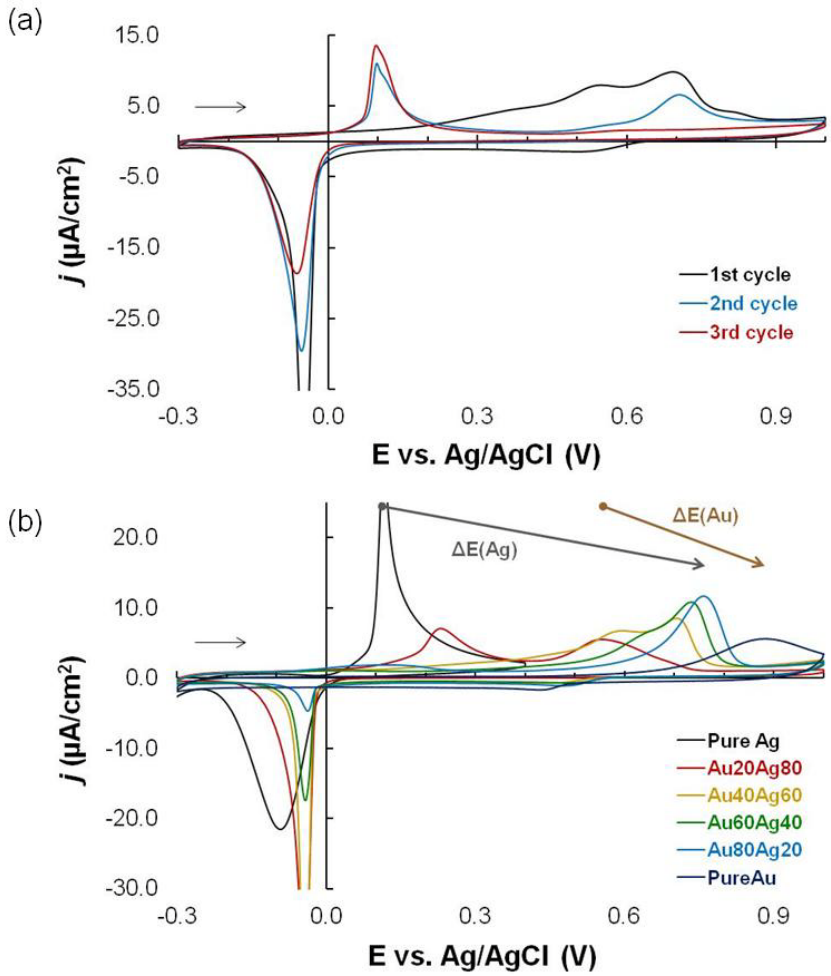

Figure 9. Cyclic voltammograms showing (a) gold-dealloying for $Au_{40}Ag_{60}$ NPs over 3 cycles (in 0.1 M NaCl) and (b) the first gold-dealloying cycles for the full range of Au_xAg_{1-x} NP compositions (in 0.1 M NaCl)

The composition of the alloy NPs also affected their gold-dealloying behavior. The first cycle of gold-dealloying in chloride for the full range of gold-silver alloy NP compositions are shown (Figure 9b). The most prominent trend was the shift in the silver-oxidation and gold-dealloying waves toward higher oxidative potentials for samples with higher gold content. It was not known if this trend was analogous to the silver-dealloying

case where the abundance of gold to block the dealloying front caused the overpotential to shift. In the gold-dealloying case, the silver-to-silver chloride phase-transition, its accompanying lattice expansion, and the highly oxidizing applied potentials were expected to mitigate the blocking effects of the gold atoms, so the mechanisms of gold-dealloying were expected to have different influences. A more plausible explanation was the extent of coordination, and therefore electronic coupling, between gold and silver in the alloy NPs tuned the electronic stability of each metal and shifted their oxidization potentials. Both silver and gold atoms with higher coordination to gold would be stabilized toward oxidation and would require a larger applied overpotential whereas silver-coordination would destabilize them toward oxidation. For the gold-rich $Au_{80}Ag_{20}$ NPs, silver-oxidation and gold-dealloying converged into a single wave signifying that both processes became coupled. Charge integration could only be performed on the well-resolved oxidation peaks for $Au_{20}Ag_{80}$ NPs, and the calculated NP composition of 22.8% Au and 77.2% Ag was in good agreement with the as-synthesized ratio. Characterization of gold-dealloyed NPs is also ongoing.

Conclusions

This project was successful in demonstrating both dealloying cases for gold-silver alloy NP-LbL electrodes. Electrochemical silver-dealloying of alloy NPs showed the silver was removed within 4 cycles and gold NPs were retained on the electrode. Alloy composition affected the silver-dealloying potential with its onset shifting to higher potentials in samples with more gold. This supported the conclusions of Sieradzki et al. in explaining this shift as the competing rates of silver dealloying and passivation of the

core by diffusing gold atoms. Electrochemical gold-dealloying showed irreversible dissolution of the gold from the NPs within 3 cycles while oxidized silver was retained as silver chloride. Silver oxidation was passivated by gold in the first scan but exhibited reversible silver/silver chloride redox behavior thereafter. The oxidation waves for each metal was comprised of two distinct oxidative processes. This was hypothesized to be the oxidation of labile surface atoms followed by protected gold-coordinated core atoms. Gold-dealloying behavior of the NPs was also influenced by alloy composition. Increased gold abundance caused oxidation of both metals to shift to higher oxidation potentials. Alloy compositions calculated from charge integration of the voltammograms were in good agreement with the as-synthesized NP compositions. These reported results contribute toward understanding the behavior of dealloying in small-scale NPs that could be developed as electrocatalysts.

Chapter 4

CHARGE-MEDIATED ELECTROCHEMISTRY OF COMPOSITE NANOPARTICLE THIN-FILMS

Introduction

A comparison of the NP surface coverages calculated from the optical absorbance of the composite thin-films showed a discrepancy with those calculated from the integrated voltammograms from the electrochemical dealloying experiments. Figure 10 shows that the percentage of alloy NPs involved in electrochemical dealloying were less than 1% of those contributing to the optical absorbance of the films. The masking of the non-active potions of the ITO electrode before LbL preparation ensured that the inactive NPs were confined to the active surface of the electrode. This could be interpreted in multiple ways. One possibility was that dealloying did not penetrate deeply into the NP cores. Although this could still potentially produce an improved catalyst by modifying the active surface, complete dealloying to leave a pure metal NP could require very long time scales. Another explanation was that a large subset of the NPs were electrochemically inactive in the film, and that electroactive NPs underwent complete dealloying. Likely, the realistic explanation involved both effects to unknown extents.

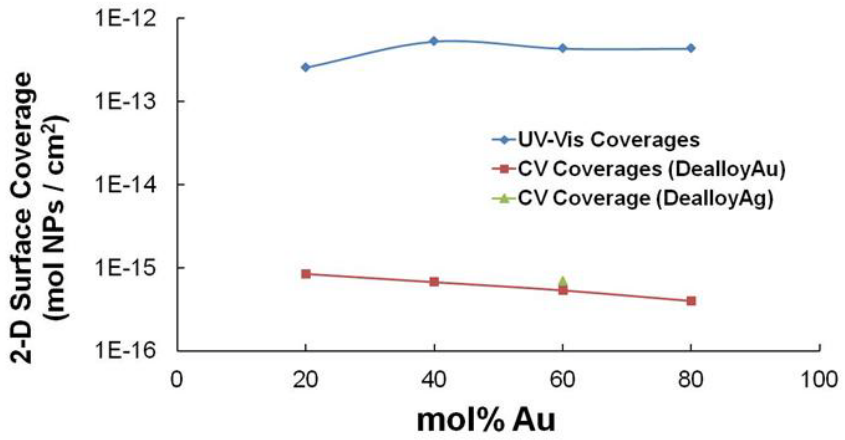

Figure 10. The surface coverages calculated from UV-Vis (diamond) and CV (squares/triangle) are compared showing that a small percentage of NPs are inactive on the LbL film

By using a solution-phase compound to mediate charge to the inactive NPs, the percentage of inactive NPs in the LbL film could be estimated assuming complete dealloying did occur. A schematic for this process is shown in Figure 11. Although this does not provide insight into the extent of dealloying in individual NPs, it does allow the fraction of inactive NPs to be determined. Further elemental studies on individual dealloyed NPs would provide additional insight into the extent of dealloying within the NP cores.

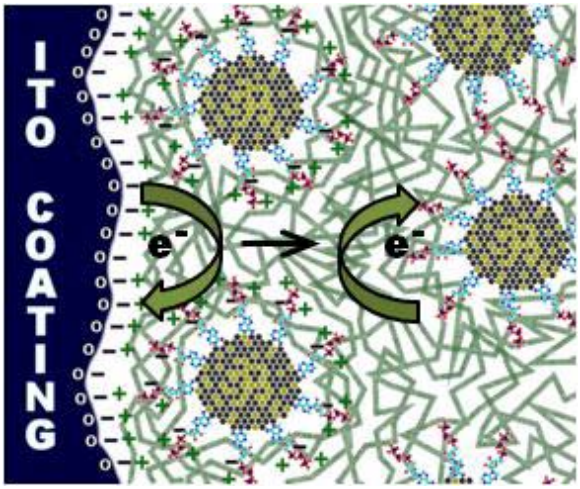

Figure 11. Schematic for the charge-mediated oxidation of NPs in LbL films on ITO. The charge-mediator used for this study was Fc(meOH) (E ≈ +200 mV vs. Ag/AgCl)[57]

Experimental

Ferrocenemethanol (Fc(meOH), 95%) was purchased from Sigma-Aldrich. The NP-LbL preparation followed the previously described methods, however, three LbL cycles were applied. The charge-mediated experiments were performed by CV with a CHI760C potentiostat (CH Instruments, Inc.) using a flame-polished Pt folded-wire counter electrode and Ag/AgCl (saturated NaCl) reference electrode (+0.22 V vs. SHE). Similar to the previous cells, electrolyte solutions were purged with N_2 for at least 20 minutes before any electrochemical experiments. The potentiostat leads were clipped to a gold foil folded over the top of the NP-LbL electrode and kept dry. The non-mediated CVs were performed in 50 mM NaCl while all of the charge-mediated experiments were done in <500 µM Fc(meOH) and 50 mM NaCl at 10 mVs^{-1} scan rate. An oxidative scan began at -0.6 V and continued to +0.8 V before it was reversed for the reductive scan.

Results and Discussion

The first charge-mediation cycles for silver NP-LbL films and the accompanying control experiments are overlaid in Figure 12. The bare ITO and ITO/PDDA voltammograms essentially overlapped and showed a single reversible wave centered at +200 mV (vs. Ag/AgCl) displaying reversible redox behavior for Fc(meOH) to Fc^{+}(meOH). Fc(meOH) was chosen as the mediator because it oxidized at higher potentials than those for silver-to-silver chloride oxidation which would favor the charge-transfer to the inactive NPs. The chosen Fc(meOH) concentration exhibited a diffusion-limited wave that was a small fraction of the silver-to-silver chloride oxidation wave ensuring that the charge-mediation wave would not be obscured. A control experiment with silver NPs in non-mediated electrolyte showed reversible silver-to-silver chloride electrochemistry typical for this NP-LbL system centered at +0 V. Using a similarly-prepared silver NP-LbL sample in the charge-mediation electrolyte, the silver oxidation peak initially correlated well with the control run. However, a secondary oxidation wave appeared at +250 mV as the oxidized Fc(meOH) served to oxidize the inactive silver NPs. The large relative currents for this wave showed the catalytic effect the inactive silver had on the Fc^{+}(meOH) as it reduced back to Fc(meOH). The concentrations of Fc(meOH) increased near the electrode due to this recycling thereby increasing the diffusion-limited currents in the oxidative wave. The reverse scan showed a small Fc^{+}(meOH) reduction wave similar to the diffusion-limited bare ITO run. Charge-transfer from the inactive silver NPs to Fc^{+}(meOH) prevented any accumulation of the oxidized species during the reduction scan. Integration of the non-mediated and mediated waves were used to estimate that 67% of the silver NPs in the film were inactive (1.7×10^{-3} C

for active silver atoms, 3.4 x 10^{-3} C for inactive silver atoms). This did not account for the full discrepancy that was observed between CV and UV-Vis surface coverages in alloy NP films, so further study must attempt to quantify the penetration depth of dealloying for a given dealloying time scale. The silver chloride reduction wave also increased in the return scan suggesting that either inactive NPs became active after mediated oxidation, or that some digestive ripening was occurring during silver oxidation causing active NPs to grow.

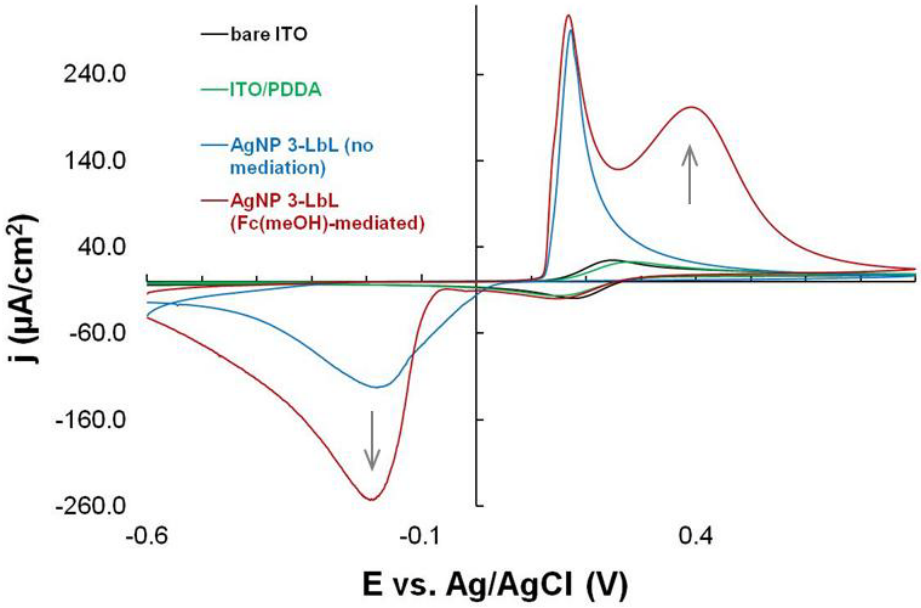

Figure 12. The charge-mediated CVs of pure silver NPs in three-layer LbL films and controls on ITO are overlaid. With the exception of the non-mediated AgNP 3-LbL voltammogram which was performed without Fc(meOH), all CVs were performed in 50 mM NaCl and <500 μM Fc(meOH) at a scan rate of 10 mVs^{-1} from -0.6 V to +0.8 V (vs. Ag/AgCl)

Conclusions

The charge-mediated experiments confirmed that inactive NPs were retained on the LbL films. Fc(meOH) transferred electrons to the electrode surface at highly oxidizing potentials, diffused away from the surface, and then oxidized the metal atoms in inactive NPs. This was verified by the appearance of an irreversible and disproportionally large Fc(meOH) oxidation wave in the charge-mediated experiments. The estimated percentage of inactive NPs in the LbL film was ~67%. Further study is needed to make definitive quantitative conclusions about the extent that NP inactivity and dealloying depth has influenced the lower-than-expected electrochemical waves coverages compared to UV-Vis surface coverages.

Chapter 5

SUMMARY

The preparation of transparent alloy NP-LbL electrodes and the demonstration of both dealloying cases for these NP films were successful. The optical analysis of colloidal solutions confirmed that spherical alloy NPs were produced with efficient formation of alloy NPs from the precursor metals without sacrificial loss of silver to silver chloride. Optical analysis confirmed the presence of alloy NPs on the LbL films, although the intrinsically low charge density on the ITO surface contributed to low NP surface coverages of ~20% ccp for saturated single-layer films. Voltammograms for silver-dealloying and gold-dealloying of the NP-LbL films both showed the expected as-synthesized atomic ratios which suggested dealloying completely penetrated the active NPs. However, comparisons of surface coverages from optical data to the electrochemical data suggested that inactive NPs were present. Charge-mediated electrochemistry of the NP-LbL films confirmed that a non-trivial percentage of inactive NPs were present in the film. Further efforts are needed to either increase the percentage of NPs that remain conductive with the electrode or to identify a feasible charge-mediator capable of oxidizing highly noble metals such as gold.

REFERENCES

[1] Liu, J. H.; Wang, A. Q.; Chi, Y. S.; Lin, H. P.; Mou, C. Y. *J. Phys. Chem. B* **2005**, *109*, 40.

[2] Wang, A. Q.; Liu, J. H.; Lin, S. D.; Lin, T. S.; Mou, C. Y. *J. Catal.* **2005**, *233*, 186.

[3] Mayrhofer, K. J. J.; Juhart, V.; Hartl, K.; Hanzlik, M.; Arenz, M. *Angewandte Chemie-International Edition* **2009**, *48*, 3529.

[4] Cochell, T.; Manthiram, A. *Langmuir* **2012**, *28*, 1579.

[5] He, W. W.; Wu, X. C.; Liu, J. B.; Zhang, K.; Chu, W. G.; Feng, L. L.; Hu, X. A.; Zbou, W. Y.; Me, S. S. *Journal of Physical Chemistry C* **2009**, *113*, 10505.

[6] Tokonami, S.; Morita, N.; Takasaki, K.; Toshima, N. *Journal of Physical Chemistry C* **2010**, *114*, 10336.

[7] Lim, D. C.; Lopez-Salido, I.; Dietsche, R.; Kim, Y. D. *Surf. Sci.* **2007**, *601*, 5635.

[8] Plieth, W. J. *J. Phys. Chem.* **1982**, *86*, 3166.

[9] Ivanova, O. S.; Zamborini, F. P. *Anal. Chem.* **2010**, *82*, 5844.

[10] Ivanova, O. S.; Zamborini, F. P. *J. Am. Chem. Soc.* **2010**, *132*, 70.

[11] Kumar, A.; Buttry, D. A. *Journal of Physical Chemistry C* **2013**, *117*, 26783.

[12] McCue, I.; Snyder, J.; Li, X.; Chen, Q.; Sieradzki, K.; Erlebacher, J. *Phys. Rev. Lett.* **2012**, *108*.

[13] Wilcoxon, J. P.; Abrams, B. L. *Chem. Soc. Rev.* **2006**, *35*, 1162.

[14] Mulvaney, P. *Langmuir* **1996**, *12*, 788.

[15] Link, S.; Wang, Z. L.; El-Sayed, M. A. *J. Phys. Chem. B* **1999**, *103*, 3529.

[16] Sanchez-Ramirez, J. F.; Pal, U.; Nolasco-Hernandez, L.; Mendoza-Alvarez, J.; Pescador-Rojas, J. A. *Journal of Nanomaterials* **2008**.

[17] Alqudami, A.; Annapoorni, S.; Govind; Shivaprasad, S. M. *J. Nanopart. Res.* **2008**, *10*, 1027.

[18] Tsai, T. H.; Thiagarajan, S.; Chen, S. M. *J. Appl. Electrochem.* **2010**, *40*, 493.

[19] Chen, D. H.; Chen, C. J. *J. Mater. Chem.* **2002**, *12*, 1557.

[20] Lu, X. M.; Tuan, H. Y.; Chen, J. Y.; Li, Z. Y.; Korgel, B. A.; Xia, Y. N. *J. Am. Chem. Soc.* **2007**, *129*, 1733.

[21] Zhang, Q. B.; Xie, J. P.; Lee, J. Y.; Zhang, J. X.; Boothroyd, C. *Small* **2008**, *4*, 1067.

[22] Ji, Y. T.; Yang, S. C.; Guo, S. W.; Song, X. P.; Ding, B. J.; Yang, Z. M. *Colloids and Surfaces a-Physicochemical and Engineering Aspects* **2010**, *372*, 204.

[23] Shibata, T.; Bunker, B. A.; Zhang, Z. Y.; Meisel, D.; Vardeman, C. F.; Gezelter, J. D. *J. Am. Chem. Soc.* **2002**, *124*, 11989.

[24] Tsuji, M.; Ogino, M.; Matsunaga, M.; Miyamae, N.; Matsuo, R.; Nishio, M.; Alam, M. J. *Crystal Growth & Design* **2010**, *10*, 4085.

[25] Zhang, Q. B.; Xie, J. P.; Liang, J.; Lee, J. Y. *Adv. Funct. Mater.* **2009**, *19*, 1387.

[26] Smetana, A. B.; Klabunde, K. J.; Sorensen, C. M.; Ponce, A. A.; Mwale, B. *J. Phys. Chem. B* **2006**, *110*, 2155.

[27] Turkevich, J.; Stevenson, P. C.; Hillier, J. *Discussions of the Faraday Society* **1951**, 55.

[28] Zhao, W. A.; Gonzaga, F.; Li, Y. F.; Brook, M. A. *Adv. Mater.* **2007**, *19*, 1766.

[29] Singh, P.; Parent, K. L.; Buttry, D. A. *J. Am. Chem. Soc.* **2012**, *134*, 5610.

[30] Kim, J. I.; Duschner, H. *Journal of Inorganic & Nuclear Chemistry* **1977**, *39*, 471.

[31] Decher, G. *Science* **1997**, *277*, 1232.

[32] Van Hyning, D. L.; Zukoski, C. F. *Langmuir* **1998**, *14*, 7034.

[33] Richards, V. N.; Rath, N. P.; Buhro, W. E. *Chem. Mater.* **2010**, *22*, 3556.

[34] Li, X. Ph.D. Dissertation, Arizona State University, 2012.

[35] Singh, P.; Buttry, D. A. *Journal of Physical Chemistry C* **2012**, *116*, 10656.

[36] Hermann, K. In *Crystallography and Surface Structure*; Wiley-VCH Verlag GmbH & Co. KGaA: 2011, p 265.

[37] Kim, K.; Kim, K. L.; Choi, J. Y.; Lee, H. B.; Shin, K. S. *Journal of Physical Chemistry C* **2010**, *114*, 3448.

[38] Zhang, H. J.; Okuni, J.; Toshima, N. *J. Colloid Interface Sci.* **2011**, *354*, 131.

[39] Huang, Y. F.; Huang, K. M.; Chang, H. T. *J. Colloid Interface Sci.* **2006**, *301*, 145.

[40] Mulvaney, P.; Giersig, M.; Henglein, A. *J. Phys. Chem.* **1993**, *97*, 7061.

[41] Liu, X. O.; Atwater, M.; Wang, J. H.; Huo, Q. *Colloids and Surfaces B-Biointerfaces* **2007**, *58*, 3.

[42] Maye, M. M.; Han, L.; Kariuki, N. N.; Ly, N. K.; Chan, W. B.; Luo, J.; Zhong, C. J. *Anal. Chim. Acta* **2003**, *496*, 17.

[43] Han, L.; Maye, M. M.; Leibowitz, F. L.; Ly, N. K.; Zhong, C. J. *J. Mater. Chem.* **2001**, *11*, 1258.

[44] Hostetler, M. J.; Zhong, C. J.; Yen, B. K. H.; Anderegg, J.; Gross, S. M.; Evans, N. D.; Porter, M.; Murray, R. W. *J. Am. Chem. Soc.* **1998**, *120*, 9396.

[45] Greeley, J.; Stephens, I. E. L.; Bondarenko, A. S.; Johansson, T. P.; Hansen, H. A.; Jaramillo, T. F.; Rossmeisl, J.; Chorkendorff, I.; Norskov, J. K. *Nature Chemistry* **2009**, *1*, 552.

[46] Stamenkovic, V. R.; Mun, B. S.; Mayrhofer, K. J. J.; Ross, P. N.; Markovic, N. M. *J. Am. Chem. Soc.* **2006**, *128*, 8813.

[47] Lai, F. J.; Su, W. N.; Sarma, L. S.; Liu, D. G.; Hsieh, C. A.; Lee, J. F.; Hwang, B. J. *Chem. Eur. J.* **2010**, *16*, 4602.

[48] Wang, D. L.; Yu, Y. C.; Xin, H. L. L.; Hovden, R.; Ercius, P.; Mundy, J. A.; Chen, H.; Richard, J. H.; Muller, D. A.; DiSalvo, F. J.; Abruna, H. D. *Nano Lett.* **2012**, *12*, 5230.

[49] Morrish, R.; Muscat, A. J. *Chem. Mater.* **2009**, *21*, 3865.

[50] Erlebacher, J.; Aziz, M. J.; Karma, A.; Dimitrov, N.; Sieradzki, K. *Nature* **2001**, *410*, 450.

[51] Wittstock, A.; Zielasek, V.; Biener, J.; Friend, C. M.; Baumer, M. *Science* **2010**, *327*, 319.

[52] Zeis, R.; Lei, T.; Sieradzki, K.; Snyder, J.; Erlebacher, J. *J. Catal.* **2008**, *253*, 132.

[53] Xu, C.; Xu, X.; Su, J.; Ding, Y. *J. Catal.* **2007**, *252*, 243.

[54] Chen, T.; Liu, Z. N.; Lu, W. J.; Zhou, X. F.; Ma, H. Y. *Electrochem. Commun.* **2011**, *13*, 1086.

[55] Starr, C. A.; Buttry, D. A. *Unpublished work*; Arizona State University: Tempe, AZ, 2013.

[56] Sieradzki, K.; Dimitrov, N.; Movrin, D.; McCall, C.; Vasiljevic, N.; Erlebacher, J. *J. Electrochem. Soc.* **2002**, *149*, B370.

[57] Sun, W. Y.; Kusukawa, T.; Fujita, M. *J. Am. Chem. Soc.* **2002**, *124*, 11570.

APPENDIX A

COPYRIGHT TRANSFER STATEMENT - SPRINGER JOURNALS

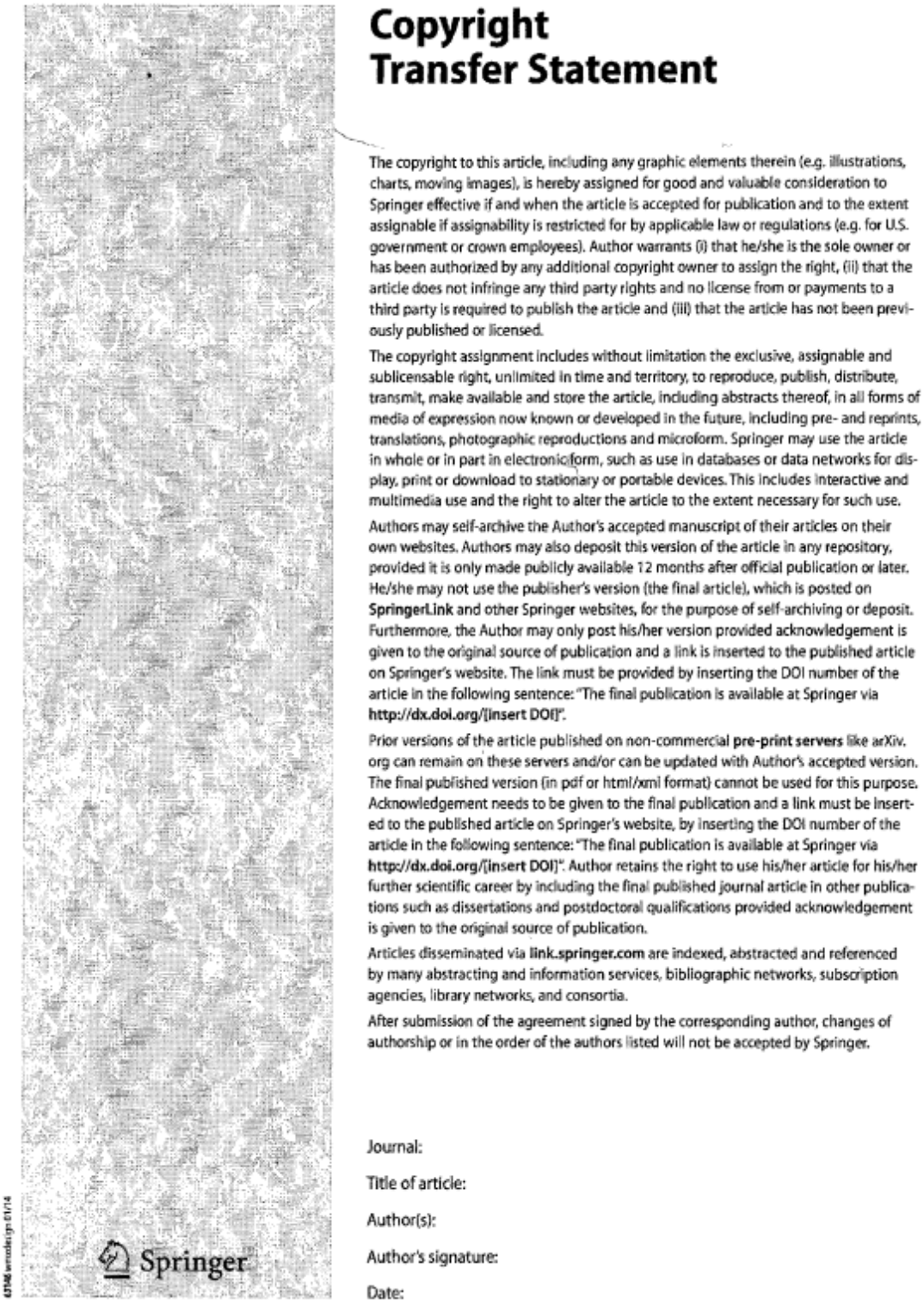

Copyright Transfer Statement

The copyright to this article, including any graphic elements therein (e.g. illustrations, charts, moving images), is hereby assigned for good and valuable consideration to Springer effective if and when the article is accepted for publication and to the extent assignable if assignability is restricted for by applicable law or regulations (e.g. for U.S. government or crown employees). Author warrants (i) that he/she is the sole owner or has been authorized by any additional copyright owner to assign the right, (ii) that the article does not infringe any third party rights and no license from or payments to a third party is required to publish the article and (iii) that the article has not been previously published or licensed.

The copyright assignment includes without limitation the exclusive, assignable and sublicensable right, unlimited in time and territory, to reproduce, publish, distribute, transmit, make available and store the article, including abstracts thereof, in all forms of media of expression now known or developed in the future, including pre- and reprints, translations, photographic reproductions and microform. Springer may use the article in whole or in part in electronic form, such as use in databases or data networks for display, print or download to stationary or portable devices. This includes interactive and multimedia use and the right to alter the article to the extent necessary for such use.

Authors may self-archive the Author's accepted manuscript of their articles on their own websites. Authors may also deposit this version of the article in any repository, provided it is only made publicly available 12 months after official publication or later. He/she may not use the publisher's version (the final article), which is posted on **SpringerLink** and other Springer websites, for the purpose of self-archiving or deposit. Furthermore, the Author may only post his/her version provided acknowledgement is given to the original source of publication and a link is inserted to the published article on Springer's website. The link must be provided by inserting the DOI number of the article in the following sentence: "The final publication is available at Springer via **http://dx.doi.org/[insert DOI]**".

Prior versions of the article published on non-commercial **pre-print servers** like arXiv.org can remain on these servers and/or can be updated with Author's accepted version. The final published version (in pdf or html/xml format) cannot be used for this purpose. Acknowledgement needs to be given to the final publication and a link must be inserted to the published article on Springer's website, by inserting the DOI number of the article in the following sentence: "The final publication is available at Springer via **http://dx.doi.org/[insert DOI]**". Author retains the right to use his/her article for his/her further scientific career by including the final published journal article in other publications such as dissertations and postdoctoral qualifications provided acknowledgement is given to the original source of publication.

Articles disseminated via **link.springer.com** are indexed, abstracted and referenced by many abstracting and information services, bibliographic networks, subscription agencies, library networks, and consortia.

After submission of the agreement signed by the corresponding author, changes of authorship or in the order of the authors listed will not be accepted by Springer.

Journal:

Title of article:

Author(s):

Author's signature:

Date:

Springer

Figure A1. Copyright transfer statement from Springer journals granting rights to republish to further scientific career in dissertations or similar publications

APPENDIX B

PERMISSION TO REPRODUCE OR RE-PUBLISH - ECS JOURNALS

Request for Permission to Reproduce or Re-Publish ECS Material

Please fax this form to: The Electrochemical Society (ECS), Attn: Permissions Requests, 1.609.730.0629. You may also e-mail your request to: copyright@electrochem.org. Include all the information as required on this form. Please allow 3-7 days for your request to be processed.

I am preparing a (choose one): ☐ paper ☐ chapter ☐ book ☒ thesis

entitled: Gold-Silver Alloy Nanoparticle Thin-Films: Preparation, Characterization and Electrochemical Dealloying

to be published by: Arizona State University

in an upcoming publication entitled: ASU Masters Theses 2014

I request permission to use the following material in the publication noted above, and request nonexclusive rights for all subsequent editions and in all foreign language translations for distribution throughout the world.

Description of material to be used—Indicate what material you wish to use (figures, tables, text, etc.) and give the full bibliographic reference for the source publication. You may attach a separate list, organized by ECS title.

Request use of FULL ARTICLE WITH FIGURES/TABLES

"Electrochemical Dealloying of Gold-Silver Alloy Nanoparticles – Selective Dissolution of the Less and More Noble Species"

Christopher A. Starr and Daniel A. Buttry

ECS Transactions, SF Meeting, Nanotechnology General Session

*Pending publication: Feb 28 2014 - A2-0163

Signature: [signature] Date: 2/22/2014

Name: Christopher Starr

Address: 732 E Vista del Cerro Dr

Tempe, AZ 85281

Telephone: 480-274-2608 Fax: N/A

E-mail: castarr@asu.edu

Permission is granted to include the above-referenced paper in your thesis, provided that you obtain permission of the other individual authors. In the thesis, please acknowledge the authors and the citation given above, and include the words: "Reproduced by permission of ECS — The Electrochemical Society."

Feb 28, 2014
Date

Ann F. Goedkoop
Ann F. Goedkoop, Director of Publications

Figure B1. Request for permission to reproduce material that is currently *in press* with *ECS Transaction* in this thesis